Polynomial Reproducing Kernel Based Image Reconstruction for ECT

Juntao Sun, Guoxing Huang(✉), Qinfeng Li, Weidang Lu, and Yu Zhang

College of Information Engineering, Zhejiang University of Technology, Hangzhou 310023, China
hgx05745@zjut.edu.cn

Abstract. Electrical capacitance tomography (ECT) is one of an electrical tomography technique, which is widely used in industrial process monitoring. It is based on multiphase flow detection and has been widely used in many fields in recent years. It is one of the research hot topics of process tomography. For purpose of improving the accuracy of ECT image reconstruction, a new image reconstruction method for ECT based on polynomial reproducing sampling kernel is put forward in this paper. Firstly, the grayscale of image is a Dirac pulse train, and it can be modeled into a discrete finite rate of innovation (FRI) model. Then, the feature information of polynomial is extracted by FRI sampling. Finally, a new observation equation is constructed by using the feature information. The original image was obtained by solving the L0 norm optimization problem. Simulations have shown that the image accuracy reconstructed by this method are better than existing algorithms.

Keywords: Image reconstruction · Electrical capacitance tomography (ECT) · Polynomial reproducing kernel · L0 norm · Finite rate of innovation (FRI)

1 Introduction

Electrical capacitance tomography (ECT) a new technology applied to multi-phase flow parameter detection [1], which can measure the material distribution of different dielectric constants by measuring the capacitance. ECT has the advantages of fast response, non-intrusion and good security [2]. Image reconstruction technology is the key to capacitance imaging application in industrial practice. Therefore, ECT technology has been developed for many years, and the research results are constantly improved and deepened [3].

The research of image reconstruction is a hot research field in recent years, and the progress is fast, and a variety of image reconstruction algorithms have been proposed [4]. The linear back projection (LBP) algorithm is the most basic and direct algorithm for ECT reconstruction. Its refactoring principle is to superimpose all the electric field lines in the induction area, and obtain the reconstructed image by solving the gray value in reverse [5]. But the image accuracy reconstructed by LBP algorithm is not enough. The image quality is lower than other algorithms when the flow pattern is complex. The

S. Shi et al. (Eds.): 6GN 2021, LNICST 439, pp. 457–469, 2022.
https://doi.org/10.1007/978-3-031-04245-4_40

Landweber algorithm can reconstruct a better image and obtain clearer image edges [6]. But Landweber uses the gradient descent method. Step size parameter problems may lead to local convergence. The quality of the image reconstructed by Tikhonov regularization algorithm has been greatly improved in the measurement center area, and an approximately stable image can be obtained [7]. The Tikhonov regularization algorithm uses the regularization solution as an approximation of the exact solution to solve the ill condition of ECT. Since this algorithm sacrifices a part of pixels in the iteration process, the image quality reconstructed by the algorithm will become worse. The Newton-Raphson algorithm obtains the least squares solution. This algorithm can reduce iteration error [7]. But the imaging speed of the algorithm is slow. The neural network algorithm is suitable for solving complex nonlinear problems [9]. But it needs to use a large number of samples, thus reducing the imaging speed. The singular value decomposition (SVD) algorithm has better reconstruction effect than LBP algorithm [10]. However, it cannot satisfy the clear reconstruction of images in the case of complex flow patterns. The algebraic reconstruction technique (ART) algorithm is better than SVD algorithm [11]. However, due to the influence of noise, the accuracy of SVD imaging needs to be improved. The Kalman filter algorithm estimates the image by iteration [11]. However, the Kalman filter algorithm takes too long because it needs matrix inversion in the iterative solution process.

In this paper, a new ECT image reconstruction method based on polynomial regenerated kernel is proposed. This method has high accuracy and correlation coefficient. First, the grayscale of image is a typical Dirac pulse train, we model the gray vector as a FRI signal. Subsequently, in the FRI sampling framework, we use polynomial reproducing kernel to filter the FRI signal. Feature extraction is carried out by uniform sampling. Finally, we combine the original data with FRI observation information. The extended sensitivity matrix and capacitance vector were reconstructed by zero filling. We rearrange the row vectors of sensitivity matrix and capacitance vector randomly, and we construct a new observation equation. The original image was obtained by solving the L0 norm optimization prob-lem. Experimental results show that this method can improve the accuracy of the image reconstruction.

The arrangement of this article is as follows: Firstly, in Sect. 2, we describe the basic principles of the ECT system. And then, in the Sect. 3, the proposed method of this paper is given. At last, based on some simulation results, we make a brief summary in Sects. 4 and 5.

2 ECT Image Reconstruction Problem

The ECT system consists of sensor array, projection data acquisition system and imaging signal processing computer, as shown in Fig. 1. Sensor systems usually consist of pairs of capacitance plates mounted uniformly on the outer walls of insulated pipes. The data acquisition device can obtain the projection data under different observation angles by measuring the capacitance values between any plate pairs, and then feed the data into the imaging computer.

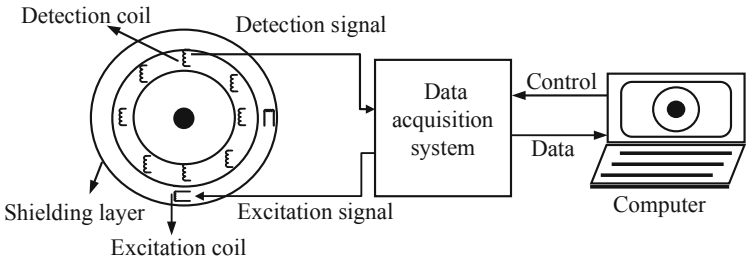

Fig. 1. The ECT system structure

2.1 The Forward Problem of ECT

The forward problem of ECT is to use some numerical analysis method to calculate the capacitance value of each electrode plate in the ECT system under the condition that the distribution of the dielectric constant in the measured area is known. We can use Maxwell's equation to describe the electromagnetic field:

$$\begin{cases} \nabla \times H = J_e + \frac{\partial D}{\partial t} \\ \nabla \times E = -\frac{\partial B}{\partial t} \\ \nabla \cdot B = 0 \\ \nabla \cdot D = \rho, \end{cases} \tag{1}$$

Here H is the magnetic field intensity, J_e is the conduction current density, E is the electric field intensity, B is the magnetic induction intensity and D is the displacement currents.

The measured field of ECT is electrostatic field, and it means that there is no isolated charge in the field. The boundary condition of the sensitive field in ECT is to measure the voltage value of the electrode. The forward problem can be generalized to the first kind of boundary value problem of Laplace equation: $\nabla \cdot (\varepsilon \cdot \nabla \varphi) = 0$. When the electrode i is excited by the electrode, the corresponding boundary conditions can be expressed as:

$$\mathrm{u}(x, y) = \begin{cases} u_0, (x, y) \subseteq \Gamma_i \\ 0, (x, y) \subseteq \Gamma_k + \Gamma_s + \Gamma_g, k = 1, 2, \ldots, 8, k \neq i, \end{cases} \tag{2}$$

where $\mathrm{u}(x, y)$ is electric potential distributions. u_0 is the excitation voltage. Γ_i and Γ_k represent the space position of the excitation and measurement electrode, Γ_s and Γ_g represent the space position of shielding layer and radial electrode.

Suppose i is the excitation electrode, and j is the detection electrode. The capacitance can be expressed as follows:

$$C_{ij} = \frac{Q_{ij}}{U_{ij}} = -\frac{\oint_\Gamma \varepsilon(x.y) \nabla \varphi(x, y) \cdot d\Gamma}{V}, \tag{3}$$

where V is the electrical potential difference between two electrodes, and Γ is the arbitrary closed curve surrounding electrode j, Q_{ij} represents the amount of charge on electrode j.

The sensitivity field is quickly calculated by the potential distribution method. The sensitivity matrix is calculated by calculating the variation of the potential in the measured region when the i and j electrodes are excitation electrodes respectively:

$$S_{ij}(k) = \frac{\triangle C_{ij}}{\triangle \varepsilon} \approx -\frac{\int_v \nabla\varphi_i \cdot \nabla\varphi_j ds}{V^2} \tag{4}$$

3 ECT Image Reconstruction Problem

The inverse problem belongs to the solution of ECT imaging problem. For the reconstruction of ECT image. Firstly, we need to obtain the known capacitance values, and then we get the sensitivity matrix of the sensitive field through simulation. Finally, we calculate the distribution of the dielectric constant of the medium in the measured area. The relationship between the dielectric constant distribution and the capacitance vector can be expressed as follows:

$$C_i = \iint_D S_i(x, y)\varepsilon(x, y)dxdy, \tag{5}$$

where D is the measured area. (5) is a nonlinear relation of integration. Therefore, the above formula requires discretization, linearization and normalization, and it can be rewritten into matrix form:

$$\mathbf{C} = \mathbf{Sg}, \tag{6}$$

where **g** is the normalized gray value vector, **C** is the normalized capacitance vector, m is the number of measured capacitance values, **S** is the normalized sensitivity matrix. and n is the number of pixels. Both m and n are integers.

The solution of (6) is the solution process of ECT inverse problem. And the number of pixels in the reconstruction area is far more than the number of capacitance values obtained, which leads to the unhealthy problem of ECT image reconstruction and the instability of the solution of ECT inverse problem. Therefore, for the sake of enhance the image reconstruction accuracy, an improved ECT image reconstruction algorithm is proposed, which is based on the use of polynomial regenerated kernel.

4 FRI Signal Modeling and Feature Extraction

In this section. What we need to do is feature extraction: Firstly, we model the gray vector as a FRI signal. In the FRI sampling system, the FRI signal is filtered by polynomial reproducing kernel and uniformly sampled. Subsequently, measurements are calculated from the samples to obtain observational feature information. Finally, the original data were combined with FRI observation information. The extended sensitivity matrix and capacitance vector were reconstructed by zero filling. We randomly rearrange the row vectors of sensitivity matrix and capacitance vector. In this way, we construct a new observation equation. The L0 norm optimization problem can be solved, so that the original signal can be recovered [13].

4.1 FRI Signal Modeling

The original image is a grayscale image composed of gray value 0 or 1. Therefore, the original signal cannot be directly sampled. We use a approximate solution to carry out FRI modeling [14]. The grayscale value of the approximate solution is between 0 and 1, which is a Dirac pulse sequence signal. So, we model the approximate solution as a typical (FRI) signal g(x):

$$g(x) = \sum_{l=0}^{L-1} a_l \delta(x - x_l), \tag{7}$$

where $x = 1, 2 \ldots, N$ is the pixel position, $x_l \in \{1, 2, ..., N\}$ is the non-zero gray value pixel position. This signal g(x) is an equally spaced signal, and can be uniformly sampled at the rate $f = \rho = 2L/n$.

4.2 Filtering and Sampling Process

In this paper, we use polynomial reproducing kernel [15]. Polynomial reproducing kernel with the order of $M - 1$ can be written as:

$$\sum_{k \in Z} \mathbf{C}_{m,k} \varphi(x - k) = x^m, m = 0, 1, \ldots, M - 1, M \in Z, \tag{8}$$

where the coefficients $\mathbf{C}_{m,k}$ can be expressed as:

$$\mathbf{C}_{m,k} = \int_{-\infty}^{\infty} x^m \, \tilde{\varphi}(x - k) dx, \;\; m = 0, 1, \ldots, M - 1; \;\; k = 1, 2, \ldots, K \tag{9}$$

Now we use this kernel to filter the FRI signal, and then we sample g(x) at the rate $f = \rho$ to extract polynomial feature information. In this way, we can get K sample values y_k. The classic FRI sampling structure is shown in Fig. 2. Filtering and sampling process can be simplified to the following formula:

$$\begin{aligned} y_k &= g(x) * h(x)|_{x=kT} \\ &= < \sum_{l=0}^{l-1} a_l \delta(x - x_l), \varphi(x/T - k) > \\ &= \sum_{l=0}^{L-1} a_l \varphi(x_l/T - k), \end{aligned} \tag{10}$$

where $< \cdot, \cdot >$ is the inner product process, T is the sampling interval. K is the total number of samples, and k = 1, 2…K is the sample label.

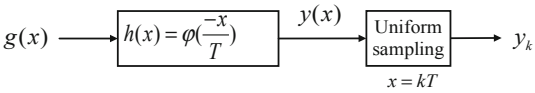

Fig. 2. Classic FRI sampling structure

4.3 Comprehensive Observation Equation

It can be known from the principle of polynomial reproducing kernel, the kernel of order $M-1$ can reproduce $M-1$ order polynomial. Measurement values can be obtained by the following formula:

$$\begin{aligned}\tau_m &= \sum_k \mathbf{C}_{m,k} y_k \\ &= \sum_{l=0}^{L-1} a_l \sum_k c_{m,k} \varphi(x_l/T - k) \\ &= \sum_{l=0}^{L-1} a_l (x_l/T)^m, m = 0, 1 \cdots, M-1,\end{aligned} \tag{11}$$

where $a_l \in [0, 1]$. The measured value u_m is expressed as a complete linear combination of all the elements in $\{1, 2, \ldots, N\}$. Assume that $u_m = \tau_m \cdot T^m$, we can rewrite the formula into the form of matrix:

$$\begin{bmatrix} u_0 \\ u_1 \\ : \\ u_{M-1} \end{bmatrix} = \begin{bmatrix} 1 & 1 & \cdots & 1 \\ 1 & 2 & \cdots & N \\ : & : & \cdots & : \\ 1 & 2^{M-1} & \cdots & N^{M-1} \end{bmatrix} \cdot \begin{bmatrix} g_0 \\ g_1 \\ : \\ g_N \end{bmatrix} \tag{12}$$

$$\mathbf{U} = \mathbf{A}\mathbf{g}, \tag{13}$$

where $\mathbf{U} = [u_0, u_1, \ldots, u_{M-1}]^T \in \mathbf{R}^{M\times 1}$ is FRI observation vector, $\mathbf{A} = \{1^m, 2^m, \ldots, N^m\}_{m=0}^{M-1}$ is FRI observation matrix, $\mathbf{g} = [g_1, g_2, \ldots, g_N]^T$ is gray vector.

There was not enough information in the original signal. We have extracted the feature information, So, we can combine the data, namely the two observation equations can be combined to get a new observation equation. The new observation equation after data fusion can be simplified to the following formula:

$$\begin{bmatrix} \mathbf{C} \\ \mathbf{U} \end{bmatrix} = \begin{bmatrix} \mathbf{S} \\ \mathbf{A} \end{bmatrix} \cdot \mathbf{g} \tag{14}$$

$$\lambda = \Phi \mathbf{g}, \tag{15}$$

where $\boldsymbol{\lambda} = [\mathbf{C}; \mathbf{U}]$ is the observation vector after data fusion, and $\boldsymbol{\Phi} = [\mathbf{S}; \mathbf{A}]$ is the Sensitivity matrix after data fusion.

In the ECT system, the number of pixels is much larger than the number of capacitance values obtained, which leads to the unhealthy problem of ECT image reconstruction and the instability of the solution of ECT inverse problem. It results in a low sampling rate, which ultimately reduces reconstruction accuracy. So, in this paper, we add capacitance values into the ECT system, through zero vector expansion method [16]. In this way, the observation equation becomes sparse, therefore, we can simplify the mathematical model of the ECT system:

$$\boldsymbol{\lambda}_{new} = \boldsymbol{\Phi}_{new}\mathbf{g}, \tag{16}$$

where $\boldsymbol{\lambda}_{new}$ is comprehensive observation vector, $\boldsymbol{\Phi}_{new}$ is comprehensive observation matrix.

4.4 Solving L0 Norm Optimization Problem

Signal sparsity can meet reconstruction requirement, but the signal is not sparse enough in the ECT system [17]. Therefore, the input signals need to be converted into sparse signals. The original signal $\mathbf{g}$ can be transformed as follows [18]:

$$\mathbf{g} = \boldsymbol{\psi}\mathbf{s}, \tag{17}$$

where matrix $\boldsymbol{\psi}$ is sparse basis, the original signal $\mathbf{g}$ is projected onto the sparse basis to get sparse vector $\mathbf{s}$.

After orthogonal transformation, the signal becomes sparse. Because of the sparsity of the signal $\mathbf{s}$, the sparse solution $\mathbf{s}$ is usually obtained by solving the L0 norm optimization problem. In this paper, we use orthogonal matching pursuit (OMP) algorithm [19] to solve this problem [20]:

$$\hat{\mathbf{s}} = \arg\ \min ||\mathbf{s}||_0 \quad s.t.\ \boldsymbol{\lambda}_{new} = \mathbf{S}_{new}\boldsymbol{\psi}\mathbf{s}, \tag{18}$$

where the L0 norm $||\mathbf{s}||_0$ represents the number of nonzero coefficients in $\mathbf{s}$. So, the estimation of the original image signal can be obtained as:

$$\hat{\mathbf{g}} = \boldsymbol{\psi}\hat{\mathbf{s}} \tag{19}$$

4.5 Process of the Method

Step 1: Initialization and normalization. The measured capacitance and the sensitivity matrix need to be normalized. The order of polynomial reproducing kernel is set to M-1.
Step 2: Input signal. The approximate solution $\mathbf{g}\mathrm{v} = \left(\mathbf{S}^T \cdot \mathbf{S} + \alpha\mathbf{I}\right) \cdot \mathbf{S}^T\mathbf{C}$ is modeled as a FRI signal g(x) by formula (7).
Step 3: Filtering and sampling. After modeled, the signal *g(x)* is filtered by polynomial reproducing kernel *φ(x)*. Then Equal interval sampling is used to extract sample information by formula (10).

Step 4: Comprehensive observation equation. Combining with formula (6) and formula (13), a FRI observation equation can be obtained by formula (14). A comprehensive observation equation is constructed by formula (16).
Step 5: Sparse solution reconstruction. In order to solve the observation equation, we can represent the signal **g** by orthogonal transformation as shown in (17). Then the L0 norm optimization problem is solved by formula (18) based on OMP algorithm.
Step 6: Image reconstruction. Finally, the ECT image can be estimated and reconstructed as formula (19).

5 Simulation Results

In order to verify the performance of the proposed method in this paper, the simulation model is carried out. The numerical simulation model was established with COMSOL software. The simulation model established is as follows: the pipe is square. The height of the pipe is 0.13 m, and the width of the pipe is 0.06 m. The thickness of the shielding layer is 0.007 m. The thickness of the pipe is 0.015 m. There are 8 measuring electrodes mounted on the four sides of the pipe, i.e. $M = 28$. The cross section of the area being measured is divided into 20×20 pixels, i.e. $N = 400$. The gray obtained by the Tikhonov regularization algorithm is modeled as a FRI signal. The polynomial sampling kernel is selected. The order of polynomial reproducing sampling kernel is 3. When the excitation voltage is applied to the excitation electrode, the potential isogram of the measured area is shown in the Fig. 3.

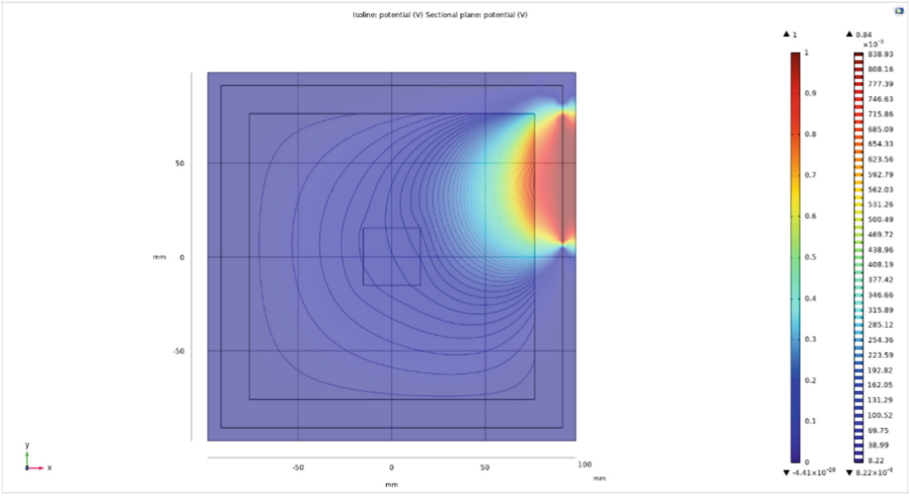

Fig. 3. The potential isogram of the measured area

The reconstructed images of the four flow patterns under different algorithms are shown in Table 1. It can be seen from the reconstruction results that the reconstructed image of the method in this paper is the closest to the original image. In general, the reconstructed image quality of the proposed method is obviously better compared with other traditional algorithms.

Table 1. The reconstruction effects of different algorithms

	(a)	(b)	(c)	(d)
Original image	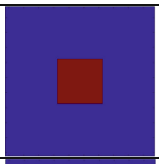	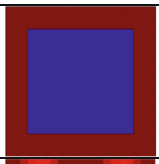	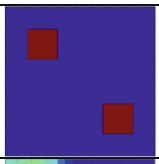	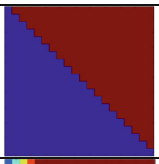
LBP	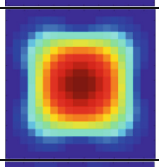	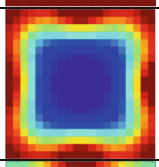	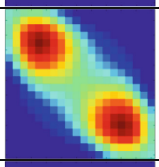	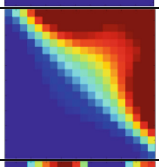
Landweber	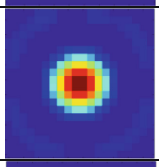	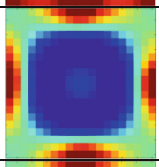	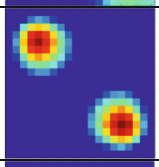	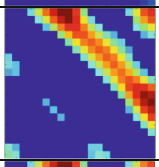
Tikhonov regularization	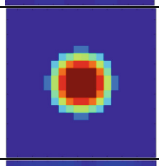	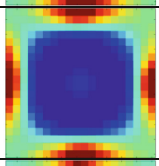	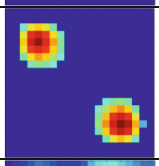	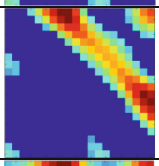
Kalman	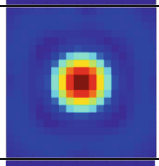	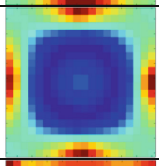	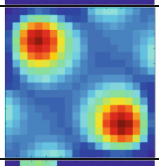	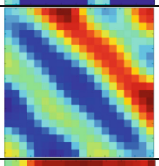
ART	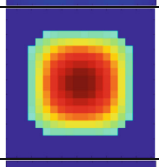	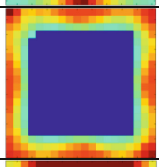	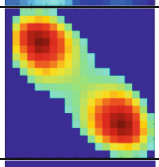	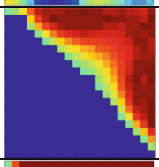
Method of this paper	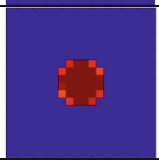	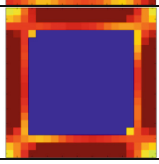	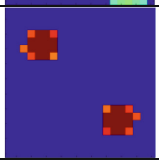	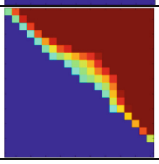

In order to qualitatively analyze the image reconstruction quality of the method in this paper, we choose to use relative error and correlation coefficient as performance indexes. The relative image error is defined as the difference degree. Image quality is inversely proportional to relative image error. The correlation coefficient is defined as the linear correlation. The higher the value, the closer the two images are, and the better the image reconstruction effect is. Tables 2 and 3 is the reconstruction image relative errors and correlation coefficients of different algorithms.

Table 2. Image errors of different algorithms

Algorithms	Flow pattern			
	(a)	*(b)*	*(c)*	*(d)*
LBP	1.2765	0.4214	1.3891	0.3118
Landweber	0.4464	0.4550	0.6476	0.7199
Tikhonov	0.4348	0.4630	0.5925	0.7198
Kalman	0.5175	0.5122	1.1745	0.5906
ART	0.8315	0.6836	0.5170	0.4874
Proposed method	0.3411	0.1742	0.2189	0.2811

Table 3. Correlation coefficients of different algorithms

Algorithms	Flow pattern			
	(a)	*(b)*	*(c)*	*(d)*
LBP	0.5725	0.8968	0.5347	0.9169
Landweber	0.9001	0.8732	0.7739	0.5759
Tikhonov	0.8936	0.8704	0.8020	0.5866
Kalman	0.8909	0.8524	0.7373	0.5959
ART	0.5474	0.9567	0.5170	0.9117
Proposed method	0.9352	0.9765	0.9736	0.9267

It can be seen from Tables 2 and 3 that the reconstructed image error of the method in this paper is much lower than other traditional algorithms, and the correlation coefficient is higher than traditional algorithms. Clearly, the images reconstructed by the proposed method have high quality and high precision. The curves of image relative errors and correlation coefficients of different algorithms are shown in the Figs. 4 and 5:

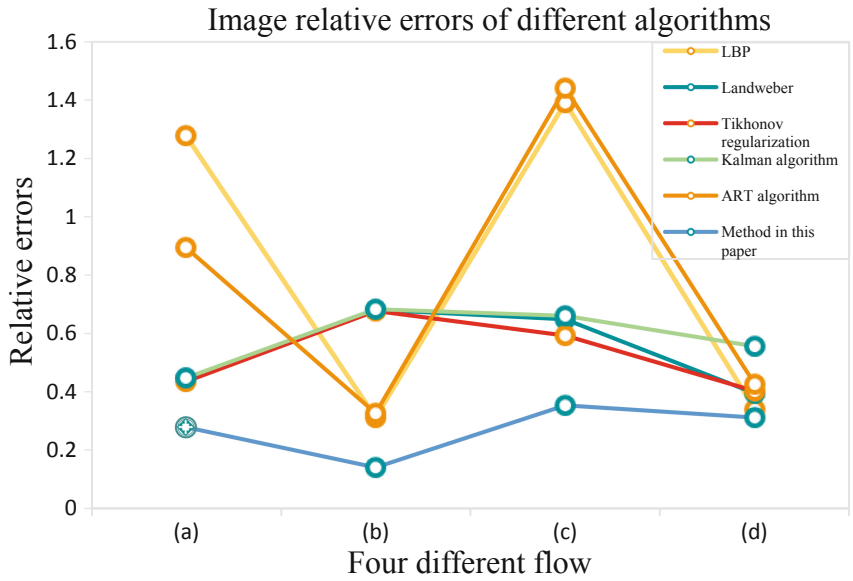

Fig. 4. The curves of image relative errors

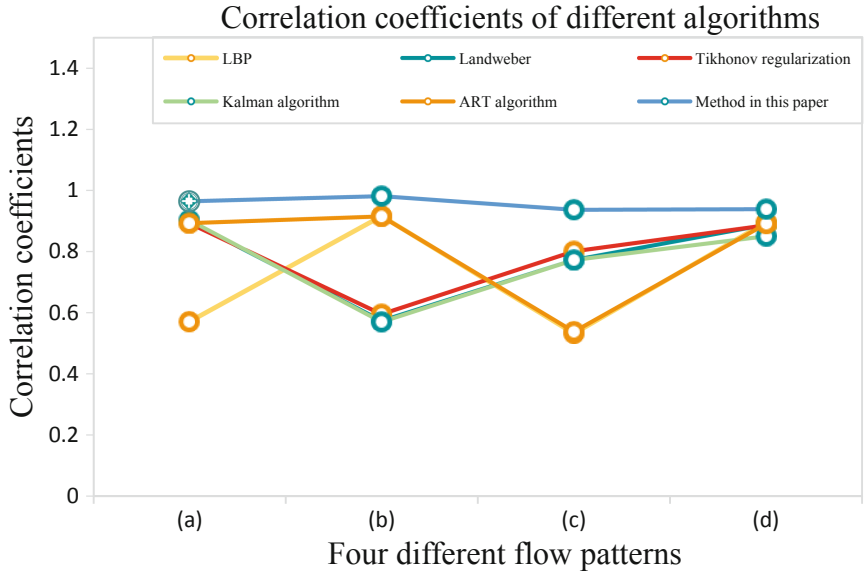

Fig. 5. The curves of correlation coefficients

6 Conclusion

Image reconstruction technology is the key to the application of capacitance imaging in industrial practice. In this paper, an ECT image reconstruction method based on polynomial reproducing is proposed to improve the image reconstruction accuracy. First, the approximate solution is modeled as an FRI signal and aligned for feature extraction. Then, a new observation equation was constructed to solve the L0 norm optimization problem to reconstruct ECT images. Simulation results have shown that compared with other existing methods, the proposed method can reconstruct the image better, and the image quality is closer to the original image. Therefore, the proposed method is effective and has better image reconstruction effect than other existing methods. On the whole, this method has a high precision of image reconstruction and is worth further study.

References

1. Meribout, M., Saied, I.M.: Real-time two-dimensional imaging of solid contaminants in gas pipelines using an electrical capacitance tomography system. IEEE Trans. Industr. Electron. **64**(5), 3989–3996 (2017)
2. Tian, Y., Cao, Z., Hu, D., Gao, X., Xu, L., Yang, W.: A fuzzy pidcontrolled iterative calderon's method for binary distribution in electrical capacitance tomography. IEEE Trans. Instrum. Meas. **70**, 1–11 (2021)
3. Sun, S., et al.: Sensitivity guided image fusion for electrical capacitance tomography. IEEE Trans. Instrum. Meas. **70**, 1–12 (2021)
4. Ji, H., et al.: A new dual-modality ECT/ERT technique based on C4D principle. IEEE Trans. Instrum. Meas. **65**(5), 1042–1050 (2016)
5. Guo, Q., et al.: A novel image reconstruction strategy for ECT: combining two algorithms with a graph cut method. IEEE Trans. Instrum. Meas. **69**(3), 804–814 (2020)
6. Ran, L., Zongliang, G., Ziguan, C., Minghu, W., Xiuchang, Z.: Distributed adaptive compressed video sensing using smoothed projected landweber reconstruction. China Commun. **10**(11), 58–69 (2013)
7. Nguyen, N., Milanfar, P., Golub, G.: A computationally efficient superresolution image reconstruction algorithm. In: IEEE Trans. Image Process. **10**(4), 573–583 (2001)
8. Wang, C., Guo, Q., Wang, H., Cui, Z., Bai, R., Ma, M.: ECT image reconstruction based on alternating direction approximate newton algorithm. IEEE Trans. Instrum. Meas. **69**(7), 4873–4886 (2020)
9. Martin, S., Choi, C.T.M.: A new divide-and-conquer method for 3D electrical impedance tomography. IEEE Trans. Magn. **54**(3), 1–4 (2018)
10. Guo, Q., Zhang, C., Zhang, Y., Liu, H.: An efficient SVD-based method for image denoising. IEEE Trans. Circuits Syst. Video Technol. **26**(5), 868–880 (2016)
11. Yao, Y., Tang, J., Chen, P., Zhang, S., Chen, J.: An improved iterative algorithm for 3-D ionospheric tomography reconstruction. IEEE Trans. Geosci. Remote Sens. **52**(8), 4696–4706 (2014)
12. Deabes, W., Bouazza, K.E.: Efficient image reconstruction algorithm for ect system using local ensemble transform kalman filter. IEEE Access **9**, 12779–12790 (2021)
13. Huang, G., Fu, N., Zhang, J., Qiao, L.: Image reconstruction method of electromagnetic tomography based on finite rate of innovation. In: 2016 IEEE International Instrumentation and Measurement Technology Conference Proceedings, pp. 1–6 (2016)
14. Mulleti, S., Seelamantula, C.S.: Ellipse fitting using the finite rate of innovationsampling-principle. IEEE Trans. Image Process. **25**(3), 1451–1464 (2016)

15. Uriguen, J.A., Blu, T., Dragotti, P.L.: FRI sampling with arbitrary kernels. IEEE Trans. Sig. Process. **61**(21), 5310–5323 (2013)
16. Ye, J., Wang, H., Yang, W.: Image reconstruction for electrical capacitance tomography based on sparse representation. IEEE Trans. Instrum. Meas. **64**(1), 89–102 (2015)
17. Ma, J., Yuan, X., Ping, L.: Turbo compressed sensing with partial DFT sensing matrix. IEEE Sig. Process. Lett. **22**(2), 158–161 (2015)
18. Hsieh, S., Lu, C., Pei, S.: Compressive sensing matrix design for fast encoding and decoding via sparse FFT. IEEE Sig. Process. Lett. **25**(4), 591–595 (2018)
19. Wang, J., Kwon, S., Li, P., Shim, B.: Recovery of sparse signals via generalized orthogonal matching pursuit: a new analysis. IEEE Trans. Sig. Process. **64**(4), 1076–1089 (2016)
20. Park, D.: Improved sufficient condition for performance guarantee in generalized orthogonal matching pursuit. IEEE Sig. Process. Lett. **24**(9), 1308–1312 (2017)